Earth and Planetary Science Letters 489 (2018) 241–250

Contents lists available at ScienceDirect

Earth and Planetary Science Letters

www.elsevier.com/locate/epsl

First quantification of relationship between dune orientation and sediment availability, Olympia Undae, Mars

Laura Fernandez-Cascales [a], Antoine Lucas [a], Sébastien Rodriguez [a,b], Xin Gao [c], Aymeric Spiga [d], Clément Narteau [a,*]

[a] Institut de Physique du Globe de Paris, Sorbonne Paris Cité, Univ Paris Diderot, UMR 7154 CNRS, 1 rue Jussieu, 75238 Paris, Cedex 05, France
[b] AIM CEA-Saclay, Université Paris Diderot, USPC, Paris, France
[c] Xinjiang Institute of Ecology and Geography, Chinese Academy of Sciences, 818 South Beijing road, Urumqi 830011, China
[d] Laboratoire de Météorologie Dynamique/Institut Pierre-Simon Laplace (LMD/IPSL), Sorbonne Université, PSL Research University, École Normale Supérieure, Université Paris-Saclay, École Polytechnique, CNRS, France

ARTICLE INFO

Article history:
Received 12 April 2017
Received in revised form 21 February 2018
Accepted 1 March 2018
Available online 12 March 2018
Editor: W.B. McKinnon

Keywords:
Mars
dunes
bedform alignment
sediment cover
aeolian transport

ABSTRACT

Dunes provide unique information about wind regimes on planetary bodies where there is no direct meteorological data. At the eastern margin of Olympia Undae on Mars, dune orientation is measured from satellite imagery and sediment cover is estimated using the high contrast between the dune material and substrate. The analysis of these data provide the first quantification of relationship between sediment availability and dune orientation. Abrupt and smooth dune reorientations are associated with inward and outward dynamics of dunes approaching and ejecting from major sedimentary bodies, respectively. These reorientation patterns along sediment transport pathways are interpreted using a new generation dune model based on the coexistence of two dune growth mechanisms. This model also permits solving of the inverse problem of predicting the wind regime from dune orientation. For bidirectional wind regimes, solutions of this inverse problem show substantial differences in the distributions of sediment flux orientation, which can be attributed to atmospheric flow variations induced by changes in albedo at the boundaries of major dune fields. Then, we conclude that relationships between sediment cover and dune orientation can be used to constrain wind regime and dune field development on Mars and other planetary surfaces.

1. Introduction

Sand seas are extensive sedimentary bodies covered by active or stable dune systems, where bedforms reflect the current or past wind regimes as well as antecedent topography, the size and shape of the basin or specific conditions of sediment supply, availability and mobility (Wilson, 1973; Wasson and Hyde, 1983; Ewing and Kocurek, 2010; Lorenz and Zimbelman, 2014). In arid regions on Earth, modern sand seas occur in major zones of deposition along sediment transport pathways arising from lacustrine, fluvial or coastal deposits. On other planets where dunes have been reported, these sources of sediment may be of different nature but, as soon as aeolian transport occurs, atmospheric circulation may be responsible for the development of sand seas over geological time scales.

Our understanding of planetary dunes is still limited by the relative paucity and, in many cases, absence of *in situ* wind measurements. This has led previous studies of dunes on Mars (Fenton et al., 2005, 2014b; Ayoub et al., 2014) and Titan (Lucas et al., 2014; Charnay et al., 2015) to rely on winds predicted by Global Climate Models (GCM) and Mesoscale Models. However, the distribution of sand flux orientation derived from global circulation or mesoscale models cannot be used alone to discriminate between different scenarios for the formation and the evolution of dune fields. Conversely, information derived from the long-term development of sand seas can be coupled with observations on the short-term bedform dynamics to obtain new estimates of the distribution of sand flux orientation, and thus important constraints on the local wind regimes (Fenton et al., 2014a, 2014b). Here, we address this specific issue in north circumpolar sand seas of Mars using orbital imagery and a new generation of model for dune growth (Courrech du Pont et al., 2014).

Martian dune fields cover an area estimated around 975,000 km^2, of which 86% belongs to the north polar region at latitudes between 68°N and 83°N (Hayward et al., 2007, 2014; Fenton and Hayward, 2010). At lower latitudes, dunes are mainly located in craters, where flow recirculations and the confined space effect are

* Corresponding author.
E-mail address: narteau@ipgp.fr (C. Narteau).

https://doi.org/10.1016/j.epsl.2018.03.001
0012-821X/

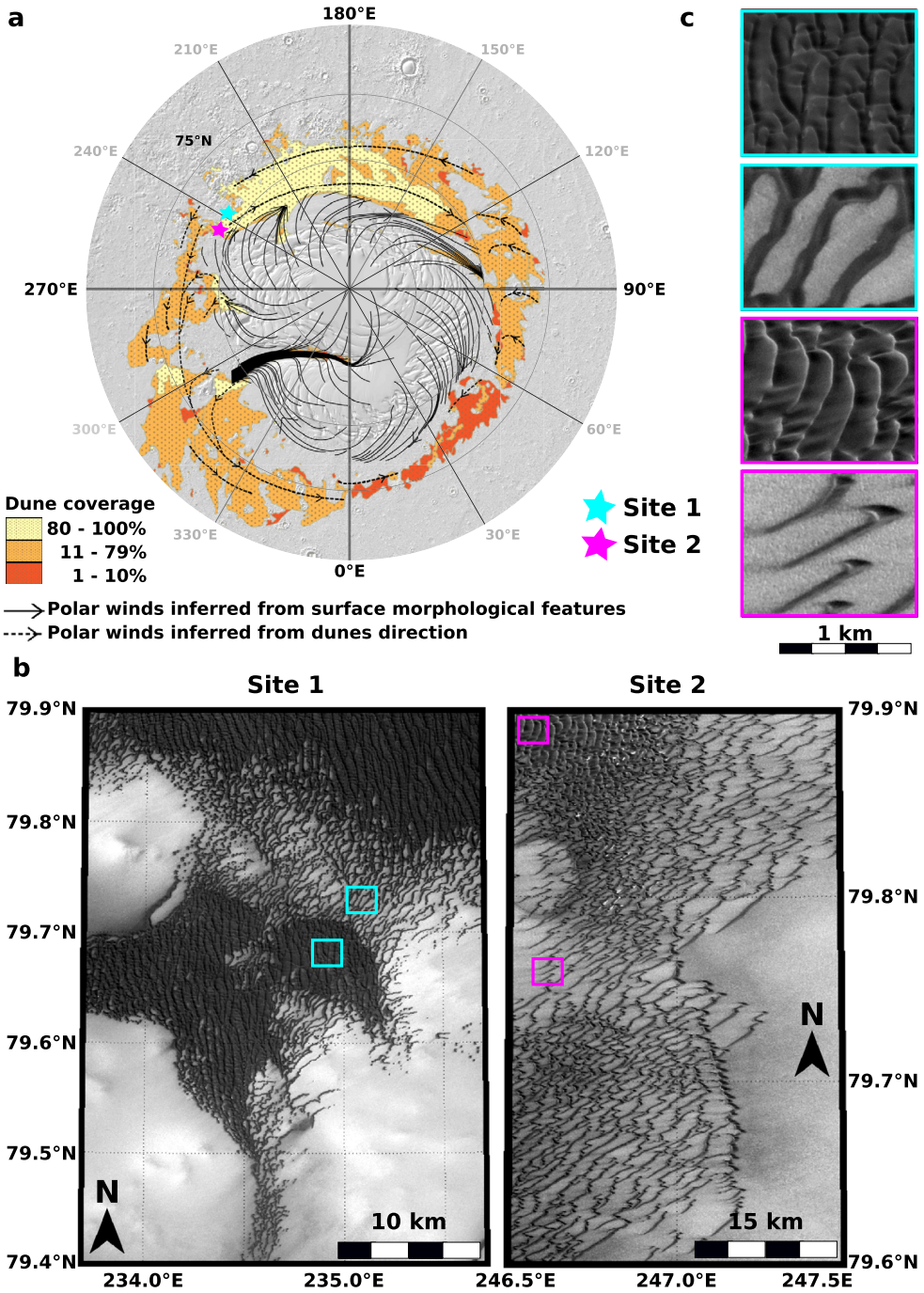

Fig. 1. Sand seas and dune systems in martian polar regions. (a) Dune fields and dune coverage around the Martian North pole. Black lines show the wind direction inferred from geomorphic features and bedforms (Massé et al., 2012). (b) Zooms on the two studied dune fields at the eastern border of the largest sand sea. (c) Zooms on specific dunes with different orientations and sediment cover in both sites.

likely to significantly affect their morphology and dynamics. For this reason, the observed dune shapes and orientations are difficult to relate to the regional wind regime or specific flow circulation patterns in craters (Fenton et al., 2005). On the other hand, the northern circumpolar region has flat or moderate topography and concentrates all the Martian sand seas (Fig. 1a), which have length scales of hundreds of kilometers.

Fifty years of Martian surface observation show that dunes are still active on Mars (e.g., Bourke et al., 2008). In polar regions, because of the seasonal CO_2 cap, transport may only occur from late spring to early fall, during approximately 30% of a Martian year (Piqueux et al., 2015). Nevertheless, modern winds on Mars are likely to continue to shape sand seas, which exhibit a limited range of dune sizes between the characteristic length scale for the formation of dunes and the giant dune size (Claudin and Andreotti, 2006; Andreotti et al., 2009). A consequence of this limited range of dune size is that, locally, most of the Martian dunes have the same age and have been shaped by winds blowing over the same time period.

The current challenges in the domain of planetary dunes are still to better evaluate the threshold wind-speed for sediment transport and to complete the current dune classification in exotic environments where sediment and fluid properties may change. However, most of these studies depend on sand flux estimates (intensity and direction), which can only be inferred from bedform dynamics. On Mars, most of these estimates are currently derived

from slip face or ripple dynamics over short time scales assuming an unidirectional wind regime (Fenton, 2006; Sullivan et al., 2008; Silvestro et al., 2010; Bridges et al., 2012; Ayoub et al., 2014). For longer time scales, considering dune patterns which cannot be explained by unidirectional wind regimes, the inverse problem determining sediment flux properties from crestline orientations has been solved using a single growth mechanism and no effect of dune shape on the flow (Fenton et al., 2014a, 2014b; Runyon et al., 2017). These studies have shown that, despite strong assumptions on the resultant sand flux direction, this is in general an under-constrained inverse problem.

An important step in the physics of sediment transport has always been to predict dune alignment in multidirectional wind regimes (i.e., from a given distribution of sediment flux orientation). At the beginning of the 1980s, the forward model simply did not exist and all studies were based on empirical evidence showing that dunes can be either perpendicular or parallel to the resultant transport direction. The model proposed by Rubin and Hunter (1987) presented a significant breakthrough in this field of research. They realized that for individual sediment flux orientation the main contribution to dune growth is the flux perpendicular to the crest. Then, they used subaqueous experiments and theory to show that, in zones of high sand availability, dunes preferentially align perpendicular to the maximum gross bedform-normal transport. This model has been successfully applied to predict bedform trend in many natural flows on Earth as well as on other planetary bodies (Rubin and Carter, 1987; Lancaster, 1991; Bourke, 2010; Rubin et al., 2008; Rubin, 2012; Fenton et al., 2014b; Lucas et al., 2014; Charnay et al., 2015; Ping et al., 2014). However, there is a also an accumulation of observations indicating that the process of dune alignment may differ (Lancaster, 2010; Gardin et al., 2012; Zhang et al., 2012). Following this line of research, recent laboratory experiments, numerical simulations and field measurements have demonstrated that a multidirectional wind regime can produce two dune trends according to sand availability (Zhang et al., 2012; Courrech du Pont et al., 2014; Gao et al., 2015b; Lü et al., 2017). As shown by Courrech du Pont et al. (2014), this is because there are two competing dune growth mechanisms:

- The bed instability mode: where there is no limit in sand availability, in transport-limited situations, dunes grow in height selecting the orientation for which the gross bedform-normal transport is maximum. Taking into account the effect of topography on wind speed, this is the model of Rubin and Hunter (1987).
- The fingering mode: where the bed is partially starved of mobilizable sediment, dunes elongates in the direction of the resultant sand flux at their crest. Where dunes grow from fixed sources of sediment, this is the orientation for which the normal-to-crest components of transport cancel each other (Lucas et al., 2015; Gao et al., 2015b).

These two distinct dune growth mechanisms determine both dune shape and orientation. Where they coexist, they can together provide two independent estimates of the sediment flux at the crest of dunes (Lü et al., 2017).

In this study, we aim to demonstrate that it is possible to provide new constraints on wind regimes from only measurements of dune orientation at places where the two dune growth mechanisms are interpreted. This is of particular interest in planetary contexts where *in situ* meteorological measurements are lacking. The next section presents the methodology employed to extract dune orientation and sediment cover in Martian polar regions from satellite imagery. This section also contains the forward model of the two dune growth mechanisms, which is used to derive two dune orientations from a distribution of sand flux orientation. Section 3 is devoted to the results obtained at two different sites, which are less than 140 km apart. The relation between dune orientation and sediment cover is discussed in Section 4 with respect to the two modes of dune orientation along sediment transport pathways. Then, solving the inverse problem of dune orientation, we present the bidirectional distributions of sediment flux orientation that can explain the observed dune shapes and alignments. From the solutions obtained in the two different sites, we discuss how our method can be systematically implemented to increase the observational dataset against which the predictions of near-surface winds of the meteorological models should be validated.

2. Methods

2.1. Imagery and dune system analysis

We analyze two dune systems in the north polar regions of Mars using images from the Context Camera (CTX) onboard the Mars Reconnaissance Orbiter (Fig. 1a). These images are calibrated and registered using the USGS Integrated Software for Imagers and Spectrometers. They serve as basemaps for mapping dune crestline with a spatial resolution of 6 m/pixel and a footprint of $\sim$ 30 km wide (Malin et al., 2007). As shown in Fig. 1b, dune material appears dark while surrounding terrains are brighter. Different dune types are observed, from linear to barchan dunes (Fig. 1c). Most importantly for the present study, interdune areas are either partially free (bright areas) or fully covered by dune material (dark areas). Throughout this article, despite the presence of regolith everywhere on Mars, we use the term "*sediment cover*" rather than dark material fractional cover to describe the proportion of dune material at the surface of the studied regions. Similarly, the regolith is described hereafter as a "*non-erodible ground*". Indeed, as shown by the loss of dune material at the horns of barchans and at the tip of linear dunes, it does not significantly contribute to bedload transport, which is the dominant mode of sediment transport on dunes.

In order to assess sediment cover, all image pixels are associated with a binary variable, dark or bright. The threshold brightness that distinguishes between these two classes is determined from the brightness distribution within each image, which is bimodal in all sites under investigation due to the high contrast between the dune material and the surrounding terrain. Then, the threshold brightness is defined as the mean of the two modal values. Sediment cover is locally computed from the ratio of dark pixels to the total number of pixels. To assign a value at each pixel, this ratio is calculated over a circle with a radius equal to the longest crest-to-crest wavelength observed in the dune system ($\approx$ 200 m).

In each image, we visually extract dune crest positions and orientations using linear segments stored and managed in Geographic Information System format for visualization and analyses. Following Lucas et al. (2014), an automatic linear segment detection has also been implemented to improve data integrity. However, given the resolution of the images, this automatic method also selects superimposed bedforms. These secondary bedforms are not in the scope of the present study because, by definition, they always occur in zone of full sediment availability (Narteau et al., 2009). Here, we concentrate only on crests of primary dunes (i.e., locally the largest bedforms), which are now characterized by a representative collection of linear segments with different orientations and lengths. In addition, only the main orientation of barchanoid bodies has been selected (i.e., the alignment of crescentic structures transverse to the resultant transport direction). To minimize the impact of subjective choices, more than 10^3 segments are identi-

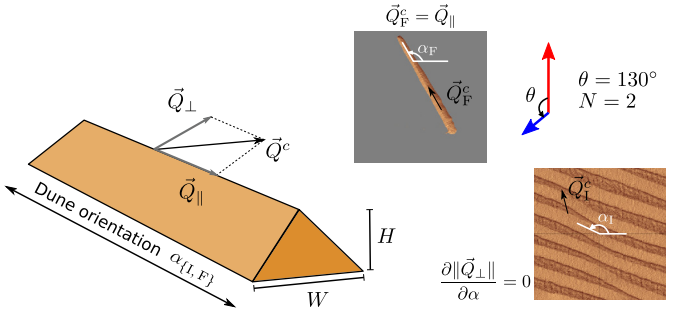

Fig. 2. Dune orientation in the bed instability and fingering modes. The resultant sand flux $\overrightarrow{Q^c}$ at the crest of a linear dune can be decomposed into two components of transport ($\overrightarrow{Q_\perp}$ and $\overrightarrow{Q_\parallel}$) according to the orientation α of the dune. In the bed instability mode, dunes select the orientation for which the normal-to-crest component of transport is maximum (i.e., $\partial\|\overrightarrow{Q_\perp}\|/\partial\alpha = 0$). In the fingering mode, dunes elongate in the direction of the resultant flux at the crest (i.e., $\overrightarrow{Q^c} = \overrightarrow{Q_\parallel}$ and $\|\overrightarrow{Q_\perp}\| = 0$). Numerical examples are extracted from Gao et al. (2015b) using a divergence angle $\theta = 130°$ and a transport ratio $N = 2$ between the two winds. The dominant and secondary winds are shown using red and blue arrows, respectively. Note that, given the speed-up effect in multidirectional wind regimes, the resultant sand flux at the crest of dunes in the bed instability and fingering modes ($\overrightarrow{Q_{\mathrm{I}}^c}$ and $\overrightarrow{Q_{\mathrm{F}}^c}$) may differ not only in intensity but also in orientation (Zhang et al., 2012; Courrech du Pont et al., 2014). (For interpretation of the colors in the figure(s), the reader is referred to the web version of this article.)

fied in each site and all the studied regions were chosen for their clear change in dune orientation (>30°).

2.2. Sediment transport at the dune crest

Dune orientations and dynamics are primarily controlled by the sand flux at the crest, which is known to differ significantly from the sand flux on a flat sand bed under the same flow conditions. For example, a positive topography accelerates the wind, so that the sediment flux over a dune depends on the dune shape. For 2D turbulent flows over low hills, the increase of wind velocity at the top of the hill, the so-called speed-up effect, is approximately proportional to the bump aspect ratio (Jackson and Hunt, 1975). Hence, at the first order of the dune aspect ratio and neglecting the transport threshold, the sediment flux at the crest of a linear dune is

$$\overrightarrow{Q^c}(\theta) = \overrightarrow{Q}(\theta)\,(1 + \gamma\,|\sin(\theta_i - \alpha)|)\,, \tag{1}$$

where α and θ are the orientation angles of the dune and of the saturated sediment flux vector $\overrightarrow{Q}$, respectively. The speed-up ratio γ writes

$$\gamma = \beta\frac{H}{W}, \tag{2}$$

where W is the width of the dune, H its height and β a dimensionless coefficient that accounts for all the other physical ingredients (e.g., roughness) that affect the speed-up. In terrestrial dune fields as well as in laboratory and numerical experiments, $\gamma = 1.6$ gives reasonable estimates of dune orientation (Gao et al., 2015b; Lucas et al., 2015; Lü et al., 2017).

2.3. Dune orientation from the distribution of sediment flux orientation

From the distribution of sediment flux orientation on a flat bed, we calculate $Q_\perp(\alpha)$, the total sediment flux perpendicular to the crest for all possible crest orientations $\alpha \in [0;\,\pi]$ (Fig. 2). The maximum value of $Q_\perp(\alpha)$ gives the most probable crest orientation α_{I} of dunes in the bed instability mode (Courrech du Pont et al., 2014; Gao et al., 2015b). For $\gamma = 0$ in Eq. (1), this is the orientation predicted by the gross bedform-normal transport rule (Rubin and Hunter, 1987). Here, by analogy with terrestrial dunes, we take $\gamma = 1.6$ to account for the increase of wind speed at the crest of dunes (i.e., the speed-up effect).

In the fingering mode, dunes elongate in the direction of the mean sediment flux at their crests. In practice, we estimate this direction by computing $Q_\perp(\alpha)$ and $Q_\parallel(\alpha)$, the total sediment flux perpendicular and parallel to the crest for all possible crest orientations $\alpha \in [0;\,2\pi]$ (Fig. 2). Then, the orientation α_{F} of finger dunes is the one for which the sediment flux perpendicular to the crest vanishes (i.e., $Q_\perp(\alpha) = 0$) and for which the flux parallel to the dune is positive (i.e., $Q_\parallel(\alpha) > 0$). If more than one solution exists, we look for the angle at which the $Q_\parallel$-value is maximum. By definition, when there is no effect of topography on the flow (i.e., $\gamma = 0$ in Eq. (1)), the orientation of the fingering mode is the resultant sediment transport direction on a flat bed. As for the α_{I}-value, the α_{F}-value depends on the γ-value when the wind speed-up is taken into account.

All sediment fluxes perpendicular to the crest contribute to dune growth. Considering the dune orientations $\alpha_{\{\mathrm{I,F}\}}$, we use the normal-to-crest component of transport to compute the characteristic growth rate $\sigma_{\{\mathrm{I,F}\}}$ of a linear dune in the bed instability or the fingering mode (Courrech du Pont et al., 2014; Gao et al., 2015b):

$$\sigma_{\{\mathrm{I,F}\}} = \frac{\int_0^{2\pi}\|\vec{Q}(\theta)\|\left(1 + \gamma\left|\sin\left(\theta_i - \alpha_{\{\mathrm{I,F}\}}\right)\right|\right)\left|\sin\left(\theta_i - \alpha_{\{\mathrm{I,F}\}}\right)\right|\mathrm{d}\theta}{2\pi\,HW}. \tag{3}$$

Basically, this is the inverse of the time required to build up a linear dune of height H and width W.

3. Dependence of dune orientation on sediment cover in north polar regions of Mars

In the boreal circumpolar region, at the eastern border of the largest Martian sand-sea (Fig. 1a), we focus on two specific dune systems located at 79.7°N, 235°E and 79.7°N, 247°E (sites 1 and 2 in Fig. 1b). These two sites occur 140 km apart and at the same latitude along the eastern edge of the Olympia Undae dune field. Both sites exhibit different dune types with various orientations (Fig. 1c), which are now analyzed with respect to changes in sediment cover along the sediment transport pathways.

Figs. 3a and 3b show the sediment cover maps of sites 1 and 2, respectively. In both cases, we span the entire range of sediment cover from 0 to 1. In site 1, a zone depleted of dune material in interdune areas separates two major sedimentary bodies (79.75°N, 234.5°E in Fig. 3a). The eastern boundaries of these major sedimentary bodies show a sharp transition from no to full sediment cover; other boundaries exhibit a more diffuse transition. In site 2, sediment cover increases to the west.

Dune crest orientation maps are shown in Figs. 3c and 3d for sites 1 and 2, respectively. The corresponding distributions of crest orientation are given in Figs. 3e and 3f. These distributions are clearly bimodal with two modes in the north–south and the 30°–210° directions. For each site, a visual comparison of dune crest orientation and sediment cover reveals potential dependence between these two variables.

For individual linear segments, Figs. 4a and 4b show the relation between sediment cover and dune crest orientation for sites 1 and 2, respectively. In both sites, there is a significant reorientation of dune alignment as the sediment cover changes. The relation takes the form of a smooth transition in site 1 and of an abrupt step in site 2. The north–south alignment is observed for full sediment cover in both sites. The other orientation is well-established for sediment cover less than 0.6 in site 2. There is more dispersion in site 1 where dunes continuously reorient as sediment cover decreases.

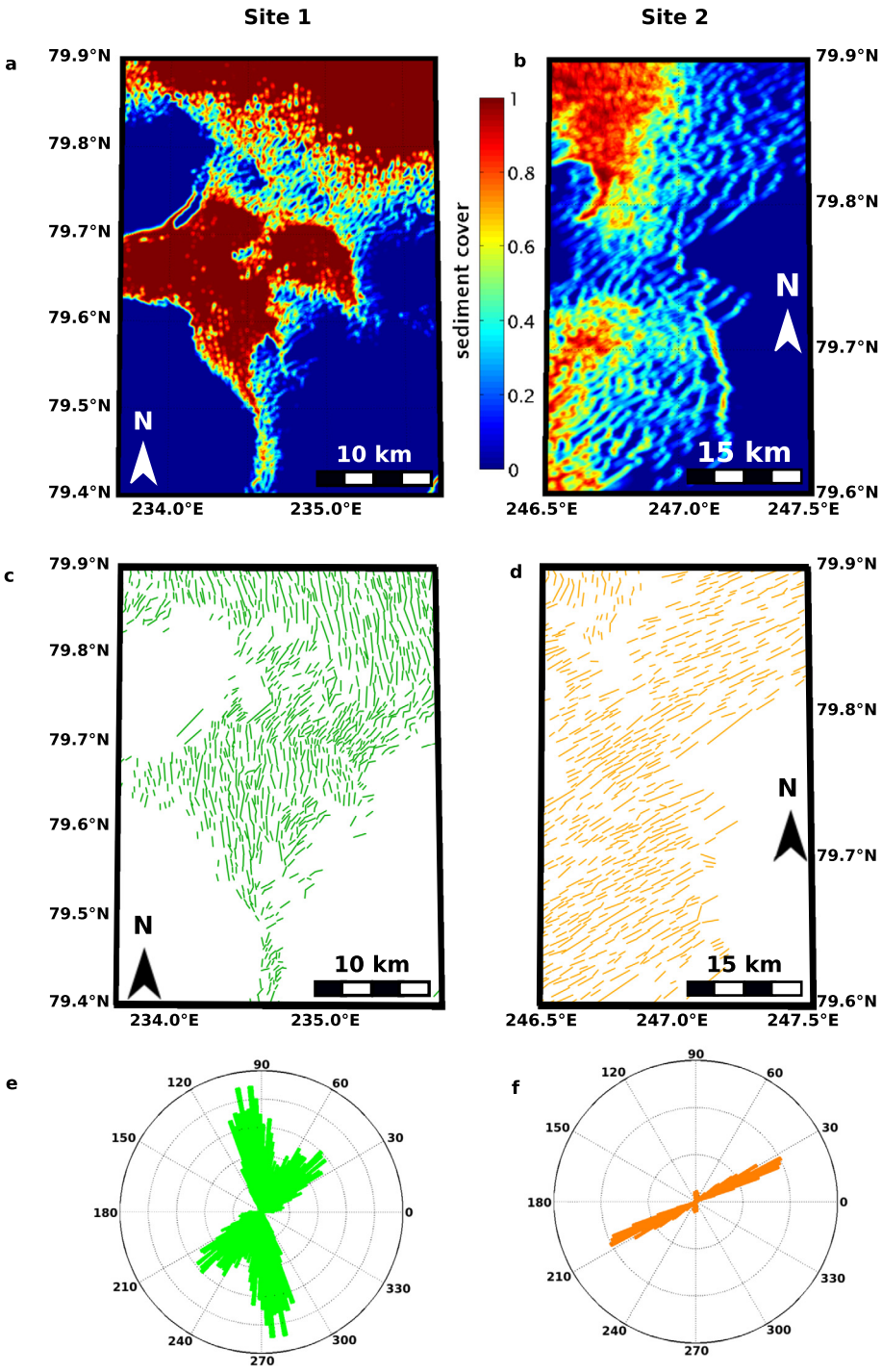

Fig. 3. Sediment cover and dune orientation in two dune systems. Site 1 (left) and 2 (right) are shown in Fig. 1b: (a, b) Mean sediment cover averaged over a distance equal to the largest wavelength observed in the dunefield (i.e., 200 m). (c, d) Crest segments manually extracted from the CTX images. Each segment is characterized by the position of its center, its length and orientation. There are 2535 and 1004 segments in sites 1 and 2, respectively. (e, f) Distribution of crest orientation.

In order to analyze the sharpness of the dune reorientation process in site 2, an error function is arbitrarily fitted to the data shown in Fig. 4b. Considering the sediment cover $0 \leq c \leq 1$ and the dune crest orientation α, it can be written as

$$\alpha(c) = a + b\,\mathrm{erf}\left(\frac{c-\mu_c}{s_c}\right), \tag{4}$$

where μ_c is the mean sediment cover at which the dune crest reorientation occurs, s_c is the rate of change in dune orientation according to sediment cover, $a = (\alpha_I + \alpha_F)/2$ and $b = (\alpha_I - \alpha_F)/2$. For site 2, the best fit to the data is obtained for $\mu_c = 0.72$, $s_c = 0.09$, $a = 235.8°$ and $b = 54.8°$ (black curve in Fig. 4b). The comparison with data indicates that Eq. (4) is well-suited for describing this dune system where there is an abrupt transitions in crest alignment and two distinct dune orientations over the two extreme ranges of sediment cover (i.e., $c \to 0$ and $c \to 1$). For a more diffuse reorientation process or if the conditions for steady-state finger dunes are not met (Gao et al., 2015b), there is no such distinct dune orientations over two different ranges of sediment cover (Fig. 4a). Nevertheless, Eq. (4) can also be used to examine the shape of the relationship between dune crest alignment

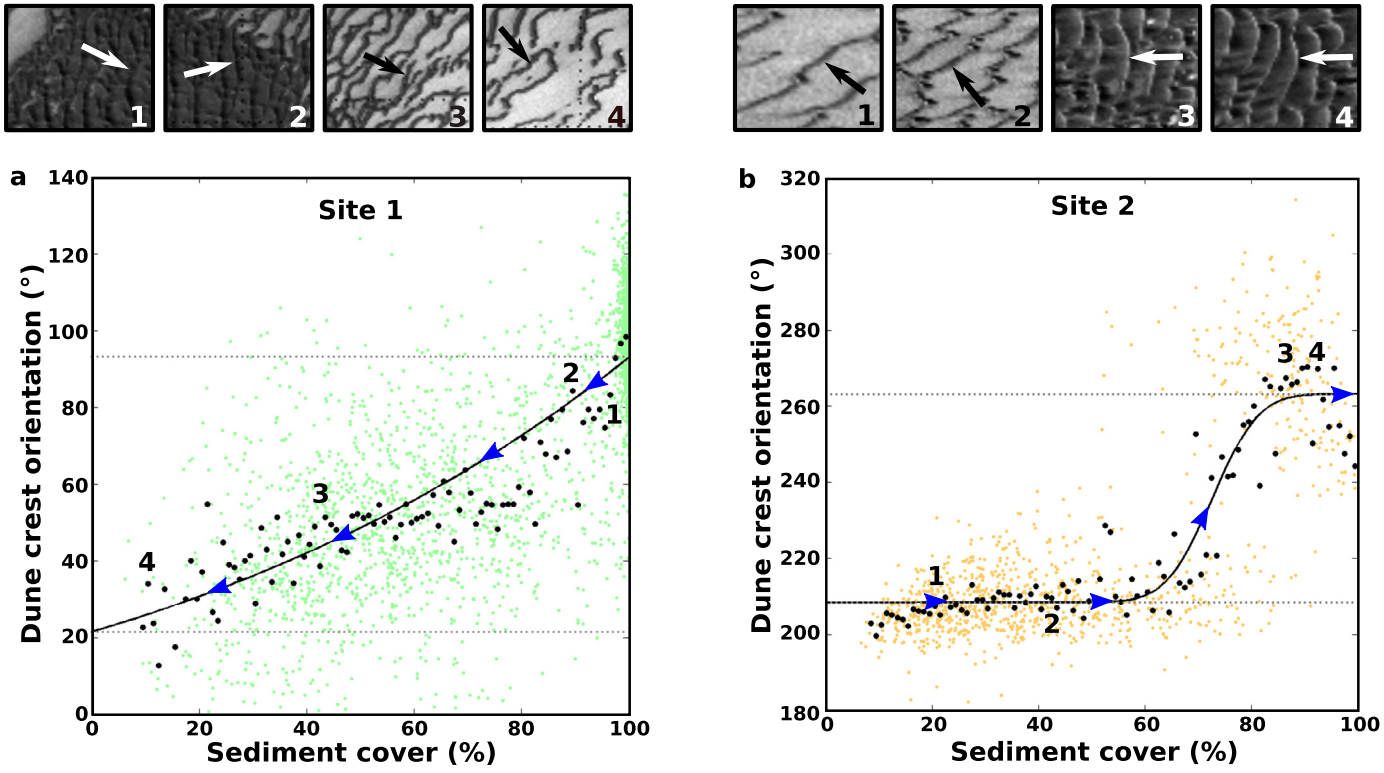

Fig. 4. Dune crest orientation with respect to sediment cover. Site 1 (a) and 2 (b) are shown in Fig. 1b. Colored dots correspond to all segments shown in Figs. 3c, d. Black dots are mean orientations computed in non-overlapping sliding windows of sediment cover with a bin width of 1%. All orientations are measured anticlockwise from east. α_I is expressed modulo π. The y-axis values are chosen according to the observed migration/elongation directions. To highlight the sharpness of the dune reorientation along the sediment transport pathways, black lines are the best fit to the data using the error function (see Eq. (4) and text for the model parameter values). Blue arrows on these curves show the dune migration/elongation directions. Dotted lines give the orientation for dunes in the bed instability (full sediment cover) and the fingering modes (no sediment cover in interdune areas). In each figure, labels and insets $\{1, 2, 3, 4\}$ show the dune segments under consideration.

and sediment cover. In this case, the parameters $\{\mu_c, a, b\}$ lose their physical meaning, but the s_c-value can still be used to evaluate the abruptness of the dune reorientation process. In addition, the two dune orientations α_F and α_I can be estimated using the α-value for $c = 0$ and $c = 1$, respectively. When Eq. (4) is tested against the data collected in site 1, the best fit gives $\alpha(0) = 93.2°$, $\alpha(1) = 21.2°$ and $s_c = 3.3$ (black curve in Fig. 4a). Then, there are two orders of magnitude difference in s_c-value between the sudden change in crest alignment observed in site 2 and the continuous change observed in site 1.

More generally, the different relationships shown in Fig. 4 can be related to the sediment transport pathways at the border of major sedimentary bodies using the migration/elongation direction of individual dunes in each dune system. It is obvious from direct observation that the dependence of dune orientation on sediment cover is not the same when individual dunes collide with or are ejected from major sedimentary bodies (Fig. 1b). This is discussed with respect to the two dune growth mechanisms in the next section.

4. Discussion

Using dune crest alignments and the high contrast between the dune material and the non-erodible ground in high latitude Martian dunefields, Fig. 4 shows how dune orientation depends on sediment cover. This is the first time that such a dependence is observed and investigated at the scale of dune systems. However, this dependence is found to be different in the two dune systems under consideration (Figs. 4a and 4b). Therefore, sediment cover is not the sole control parameter for dune orientation; dune-field boundary conditions and the long-term erosion/deposition rates along the sediment transport pathways also exert control over the development of dune patterns (Kocurek and Lancaster, 1999; Ewing and Kocurek, 2010). For this reason, sediment cover and crest alignment should be considered as two conjugate outcomes of dune growth and dynamics in areas where sand availability and supply are continuously evolving. Here, we start to document these dune patterns taking advantage of recent advances in the physics of dunes.

4.1. Two modes of dune orientation at the borders of major sedimentary bodies

Based on two dune growth mechanisms, the new generation dune model proposed by Courrech du Pont et al. (2014) provides a natural framework to analyze relations between sediment cover and dune alignment. Indeed, the fingering and the bed instability modes represent potentially the two end-members for dune orientation considering systematic changes in sand availability along the sediment transport pathways.

In zones of full sediment cover, dune crest alignment has first to be associated with the bed instability mode. In zones where interdune areas are free of sediment, dune shape and orientation depend on the dune-height growth-rate ratio σ_F/σ_I and on specific sediment availability conditions (Gao et al., 2015b). As a consequence, dune systems in areas with low sediment cover may not always exhibit longitudinal bedforms with the orientation of the fingering mode. Instead, barchan dunes or isolated bedforms with no specific trend or apparent slip face could be reported (e.g. dome dunes, whalebacks). Finally, in zones where sediment cover varies, a systematic transition from one mode of dune orientation to the other can be expected. Here we find that this transition can take different forms, and that it is necessary to account for the migration/elongation direction of dunes in order to differentiate between

zones of decreasing or increasing sediment cover. These migration directions are well-identified in the field because the characteristic time required to reshape a dune is generally few orders of magnitude larger than the characteristic time scale associated with individual winds.

In the dune system of site 2, asymmetric barchans with arms elongated northeast–southwest migrate on a non-erodible ground to ultimately collide with and merge into a major sedimentary body composed of linear bedforms with a north–south orientation. Such a coexistence of dune types and trends is a simple and illustrative example of the simultaneous expression of the two dune growth mechanisms in a multidirectional wind regime. In this particular case, there is an abrupt change in sediment cover, which is associated with spontaneous change in dune orientation. This is possible because, upstream of the major sedimentary body in a zone of low sediment cover, isolated dunes elongate and migrate along the direction of the fingering mode. Within the major sedimentary body, dunes grow from the underlying sediment layer to align along the direction of the bed instability mode. As the finger dunes are smaller and migrate in the direction of the major sedimentary body, collisions are responsible for the transition in dune alignment. The sharpness of this transition can be ascribed to the collision-type events but also to the significant difference in orientation between the involved dunes ($\approx 55°$). The sediment of the impacting finger dunes is simply redistributed on the upstream slopes of the impacted dunes in the bed instability mode, with no effect on their shape and orientation. Similar collisions and coalescences into downstream dominant bedforms have been described before under unidirectional wind regimes for barchan and transverse dunes (Gao et al., 2015a). The originality of the present collision-coalescence process is that it occurs under multidirectional wind regimes at a border of a major sedimentary body between dunes with different orientations. As shown in Fig. 4b, such conditions are associated with a step-like relation between dune orientation and sediment cover.

The dune system studied in site 1 differs substantially from the previous example. Site 1 illustrates how major sedimentary bodies expand into the surrounding areas through the dynamics of dunes. Within the main sedimentary bodies, a north–south dune orientation compatible with the bed instability mode prevails. On the eastern borders of these dune fields, linear dunes exhibit a continuous clockwise reorientation as they migrate toward zones of lower sediment cover. Those that separate from the main sedimentary bodies tend to align at 30° anticlockwise from east before breaking-up in smaller barchan dunes, which eventually disappear. Under the combined action of multidirectional wind regimes and conditions of reduced sediment availability, these transitions in both dune shape and orientation may reflect a systematic evolution from the bed instability mode to the fingering mode and trains of barchan dunes. This interpretation is supported by the relation between dune orientation and sediment cover (Fig. 4a), from which the dune alignments associated with the two dune growth mechanisms can be estimated. Nevertheless, between these two extreme values, all dune orientations can be observed.

Why is there such a smooth transition in dune orientation and not an abrupt change between the two modes predicted by the theory? Three main reasons may be invoked. The first is related to the dynamics of isolated dune tips. As the concave-downwind shape of barchans, dunes in the bed instability mode at the border of the main sedimentary body may have their crestlines that continuously reorient toward the resultant transport direction where their tips start to migrate on the non-erodible ground (see type *A* in Fig. 5). The second reason is related to the creation, interaction, and destruction of crest terminations, the so-called defects, which are the drivers of any bedform reorientation (Werner and Kocurek, 1997). When these defects are migrating across the dune

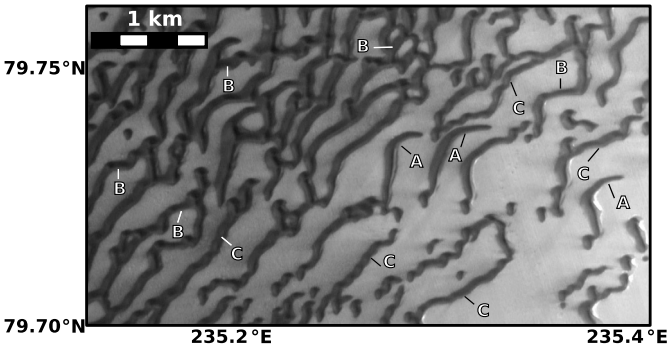

Fig. 5. Dune patterns in zone of bedform reorientation. At the border of a major sedimentary body in site 1, three types of dune behavior explain the smooth transition in dune orientation: *A*, reorientation of isolated dune tips; *B*, defect migration through a collision-ejection mechanism; *C*, Migration and elongation of dunes.

field through a collision–ejection mechanism (Gao et al., 2015a), they all propagate and align in the direction of the sediment flux at the crest of dunes in the bed instability mode, a direction that is close to both the orientation of the fingering mode and the resultant transport direction on a flat surface (see type *B* in Fig. 5). The third reason is related to the migration and the collision of isolated dunes after their ejection. Because the sources of sediment from which they elongate are mobile and moving in the direction of the sediment flux at the crest of dunes in the bed instability mode, they align along an intermediate direction between the directions associated with the two dune growth mechanisms (see type *C* in Fig. 5). In addition, as they collide with each other, they may also produce transient orientations.

Together, the field examples studied in Figs. 4a and 4b reflect the diversity of dune shape and orientation that could be produced by multidirectional wind regimes where sediment cover is not uniform in space and time. At the boundaries of major dune fields, we can now distinguish two main features from the relation between dune orientation and sediment cover:

1. Inward migration of finger dunes (Fig. 4a) where the resultant sediment flux is oriented from areas of low to high sediment cover.
2. Outward elongation of finger dunes (Fig. 4b) where the resultant sediment flux is oriented from areas of high to low sediment cover.

Most importantly, in order to provide new constraints on local climate conditions, these dune patterns may be analyzed to reconstruct the wind regimes responsible for their formation and their stability.

4.2. The inverse problem of dune orientation

The inverse problem of dune orientation consists of reconstructing the wind regimes that could have shaped the observed dune systems (i.e., dune types, orientations and dynamics). Without any assumptions on the underlying transport law, this problem reduces to determining the distribution of sediment flux orientation. Unfortunately, a complete search is not computationally feasible given the space of possible distributions. In this preliminary work, we consider only bidirectional wind regimes to investigate simple solutions particularly relevant for seasonal atmospheric variations. Under this assumption, the parameter space is restricted to the orientation Θ_N of the primary sediment transport direction (i.e., the direction of the dominant wind) as well as the angle of divergence Θ and the transport ratio N between the primary and secondary sediment transport directions (i.e., between the two winds).

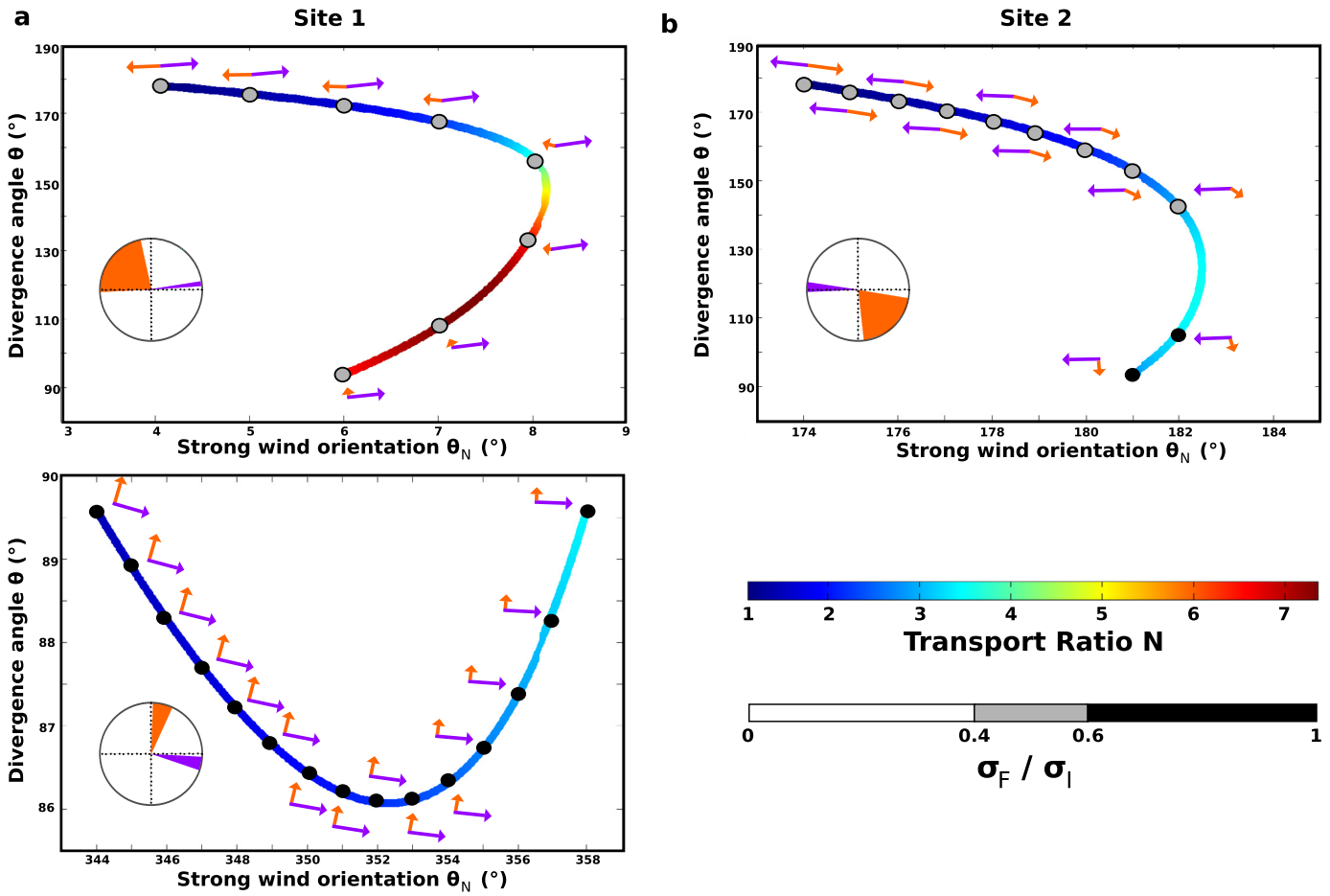

Fig. 6. Solutions of the inverse problem of dune orientation. Site 1 (a) and 2 (b) are shown in Fig. 1b. Considering only bidirectional wind regimes and the model of Courrech du Pont et al. (2014), each figure shows the distributions of sediment flux orientation that can produce the observed dune alignments (dotted lines in Fig. 4). The transport ratio N is shown by the color along the trajectories of the solutions in the parameter space $\{\Theta_N, \Theta\}$, where Θ_N is the orientation of the primary sediment transport direction and Θ the divergence angle between the two sediment transport directions. To illustrate these solutions, arrows show the corresponding sediment flux vectors. Violet and orange vectors correspond to the primary and secondary sediment transport directions, respectively. The length of the vector associated with the primary direction is normalized. Using the same color code, roses show the range of solutions for the primary and secondary sediment transport directions. To inject some constraints from dune shape into the inverse problem, gray dots show the σ_F/σ_I-value for different solutions of the inverse problem. Note the differences in σ_F/σ_I-values for the two ranges of solutions in site 1.

The input data of the inverse problem are the orientations $\{\alpha_I, \alpha_F\}$ associated with the two dune growth mechanisms. Contrary to the approach of Fenton et al. (2014a), there is no assumption on the resultant sediment flux direction. Instead, to account for the full dynamics of the dune systems under investigation, dune alignments are extracted from the relations between dune trend and sediment cover (Fig. 4): α_I is the dune orientation of the bed instability mode observed in zones of full sediment cover (i.e., 100%); α_F is the dune orientation of the fingering mode observed in zones with no sediment cover in the interdune areas (i.e., $\rightarrow$0%). As shown by the dashed lines in Fig. 4, we have $\{\alpha_I, \alpha_F\} = \{93.2°, 21.6°\}$ and $\{263.2°, 208.4°\}$ for sites 1 and 2, respectively. All orientations are measured anticlockwise from east. The orientation of dunes in the bed instability mode is expressed modulo π. For dunes in the fingering mode, α_F-values are chosen according to the observed migration/elongation direction. We do not consider any dispersion of the input data and limit the resolution of the inverse problem to single $\{\alpha_I, \alpha_F\}$-values using the model proposed by Courrech du Pont et al. (2014) with $\gamma = 1.6$ (see Sec. 2.2).

Using this forward model, a given set of $\{\Theta_N, \Theta, N\}$-values leads to an unique solution for the $\{\alpha_I, \alpha_F\}$-values. The inverse problem is less straightforward because, for a given dune growth mechanism, a specific dune orientation corresponds to wide regions of the $\{\Theta_N, \Theta, N\}$ parameter space. Considering together the two dune growth mechanisms represents a precious advantage for limiting the number of solutions. Indeed, each orientation $\alpha_{\{I,F\}}$ provides an independent set of solutions in the $\{\Theta_N, \Theta, N\}$ parameter space, so that the possible distributions of sediment flux orientation reduce to the intersections of the solutions for α_I and α_F.

Fig. 6 shows the solutions of the inverse problem of dune orientation for bidirectional wind regimes. In both sites, the narrow ranges ($\approx 15°$) of solutions for the primary sediment transport direction demonstrate the feasibility of the approach and the gain in accuracy with respect to methods based only on the bed instability mode (Fenton et al., 2014a, 2014b). Nevertheless, the ranges of divergence angle remain large (i.e., $90° < \Theta < 180°$). In this case, dune shape and the stability of finger dunes may help in reducing again the number of solutions.

Gao et al. (2015b) have shown that, in zones of low sediment availability, there are systematic transitions from linear dunes to trains of barchan dunes in the parameter space of the bidirectional wind regimes. These different types of dunes may be related to the magnitude of the dune-height growth rate ratio σ_F/σ_I: steady-state finger dunes are observed for $\sigma_F/\sigma_I > 0.6$; trains of barchans for $\sigma_F/\sigma_I < 0.4$. From the computation of this ratio for the solutions of the inverse problem, we can exclude solutions for which the observed dune shape and the σ_F/σ_I-value disagree. For example, in

site 1, the finger dunes growing from the eastern boundaries of the main sedimentary bodies are not in a steady-state. They break up in small barchan dunes, which ultimately disappear. Then, we can rule out the distributions of sediment flux orientation for which $\sigma_F/\sigma_I > 0.6$. In site 1, we can therefore eliminate all solutions for which the divergence angle Θ is smaller or close to 90° (i.e., black dots in Fig. 6a). In site 2, no solution can be excluded as they all have σ_F/σ_I-values of over 0.4 (Fig. 6b), which are consistent with the development of asymmetric barchans and the stability of their elongated horn.

Finally, the resolution of the inverse problem of dune orientation indicates that the most probable bidirectional wind regimes are dominated by zonal winds in both sites. Nevertheless, if the zonal component always dominates, there is an orientation change of 180° in the resultant sediment transport direction between the two sites separated by less than 140 km. The solutions of the inverse problem of dune orientation show that such a reversal depends only on the fine balance between the eastward and westward components in the distribution of sediment flux orientation (Fig. 6). Then, it does not require a major change in wind regime.

4.3. Constraining surface wind regimes from dune physics

The main result of this study is to show that the method based on the two dune growth mechanisms can now provide new quantitative constraints about wind regimes that have shaped dune systems on Mars, currently or in the past.

In absence of observational time series of the dunes under consideration, we cannot yet estimate the magnitude of the sediment flux at their crest from their dynamics, as has been done on Earth and Mars from the migration of dunes in the bed instability mode and/or the elongation of dunes in the fingering mode (Bridges et al., 2012; Lucas et al., 2015; Lü et al., 2017). Hence, modern transport rates in polar regions of Mars will be the subject of a forthcoming study. Nevertheless, the distinct dune morphologies as well as the presence of wind streaks at their tips and on the surrounding terrain are strong arguments for the modern activity of the dune systems under consideration.

Given the seasonal cycle on Mars, the inverse problem of dune orientation is solved only for bidirectional wind regimes. This method is not restricted to two transport directions and it has broader applicability to more general multidirectional wind regimes. However, in this case, the dimension of the parameter space could become so large that it may be necessary to add more constraints about dune dynamics (e.g., dune speed, sediment flux at the crest). In addition, the model of dune crest alignment can also be revisited to adopt more complex dune geometries and the evolution of dune shape during periods of constant wind orientation.

In north polar regions of Mars, we find here that the sediment fluxes are mainly associated with easterly and westerly winds, which may compensate each other almost completely. Then, at the eastern border of the largest sand sea on Mars, the observed convergence of dunes can be related to zonal winds and two sediment transport pathways facing each other approximately 180° apart. Such a confluence is likely to be related to conditions of deposition, suggesting a potential eastward expansion of the sand sea.

Here we show that dunes can provide information about subtle variations of the distribution of sediment flux orientation. Our method should be extended to other Martian dune fields to obtain from dune orientations a more global description of wind characteristics and aeolian transport. These characteristics can then be compared to the results of GCMs and, on specific sites of interest, mesoscale models to get insights into the interplay between global and regional circulations, which give rise to the wind regimes recorded in dune fields. The necessity of using a multiscale hierarchy of meteorological models from GCM (e.g., Forget et al., 1999) to mesoscale models (e.g., Spiga and Forget, 2009) to solve the inverse problem of dune orientation is clear from existing terrestrial and Martian dune studies. Even on Earth, the prediction of GCMs using data assimilation are not always in perfect agreement with the measured wind properties, especially in desert areas (Ping et al., 2014; Gao et al., 2015b).

Polar regions on Mars are particularly relevant examples of this interplay between global and mesoscale circulations, such as the regional flows forced by the topography or by the temperature contrast between the ice cap and the ground. Hence our conflicting results for wind directions on sites about a hundred kilometers apart is the best illustration of the perspectives opened by our new method to infer possible wind directions from dune orientations. The predominance on a global scale of a zonal circumpolar jet in polar regions of Mars is well established (Waugh et al., 2016; Toigo et al., 2017), but polar regions are also prone to mesoscale circulations with wind directions distinct from the global-scale tendency.

In addition to katabatic winds in north polar regions, polar transient eddies and thermally-direct circulations driven by ice–soil contrasts could explain the changes in distribution of sand flux orientation derived from dune shape (Toigo and Richardson, 2002; Tyler and Barnes, 2005; Smith et al., 2015). For example, these atmospheric processes could explain the systematic migration of isolated finger dunes toward the sand sea. Given the change in albedo associated with this major sedimentary body, dune fields themselves may have an influence on wind dynamics. Indeed, lower albedo may generate horizontal pressure gradients promoting the convergence of winds to areas of full sediment cover. This feedback of dune systems on the wind regime could naturally explain the subtle differences in distributions of sand flux orientation responsible for the convergence of dunes and the development of sand sea.

5. Conclusion

The contrast between the dune material and the surrounding terrain in north polar regions of Mars allows us to quantitatively analyze the dependence of dune orientation on sediment cover. It offers an unique opportunity to document the coexistence of two dune growth mechanisms in multidirectional wind regimes. We can now explain the origin of abrupt and smooth changes in dune orientation using inward and outward migration dynamics of finger dunes along sediment transport pathways. In addition, the two dune growth mechanisms can together reduce the degeneracy of the inverse problem of dune orientation, which aims at determining the distribution of sand flux orientation (i.e., the wind regimes) from dune trends. Having established the feasibility of the approach in two sites, it can be generalized across large dune systems to reconstruct sediment transport properties in places where direct meteorological measurement are lacking. This is obviously the case on Mars and Titan, the largest moon of Saturn, but also in remote desert areas on Earth where dunes might be used more effectively to document local wind regimes.

Acknowledgments and data

No author declares conflicts of interests. Authors thank S. Courrech du Pont for his thoughtful comments on the manuscript as well as S.C. Brothers and an anonymous reviewer for their constructive remarks. Author acknowledge the financial support of the UnivEarthS Labex program at Université Sorbonne Paris Cité (ANR-10-LABX-0023 and ANR-11-IDEX-0005-02), the ANR EXODUNES (ANR-12-BS05-001/EXO-DUNES), the ANR SONO (ANR-17-CE01-0014-03), Space Campus from Université Paris

Diderot, the Nvidia Academic Research Support program, the Xinjiang Uygur Autonomous Regions (High-level talents of China, no. Y742071001), the Institut Universitaire de France as well as the CNES.

References

Andreotti, B., Fourrière, A., Ould-Kaddour, F., Murray, B., Claudin, P., 2009. Size of giant dunes limited by the depth of the atmospheric boundary layer. Nature 457, 1120–1123.

Ayoub, F., Avouac, J.-P., Newman, C., Richardson, M., Lucas, A., Leprince, S., Bridges, N., 2014. Threshold for sand mobility on Mars calibrated from seasonal variations of sand flux. Nat. Commun. 5, 5096.

Bourke, M., Edgett, K., Cantor, B., 2008. Recent aeolian dune change on Mars. Geomorphology 94, 247–255.

Bourke, M.C., 2010. Barchan dune asymmetry: observations from Mars and Earth. Icarus 205, 183–197.

Bridges, N., Ayoub, F., Avouac, J., Leprince, S., Lucas, A., Mattson, S., 2012. Earth-like sand fluxes on Mars. Nature 485, 339–342.

Charnay, B., Barth, E., Rafkin, S., Narteau, C., Lebonnois, S., Rodriguez, S., Du Pont, S.C., Lucas, A., 2015. Methane storms as a driver of Titan's dune orientation. Nat. Geosci. 8, 362–366.

Claudin, P., Andreotti, B., 2006. A scaling law for aeolian dunes on Mars, Venus, Earth, and for subaqueous ripples. Earth Planet. Sci. Lett. 252, 30–44.

Courrech du Pont, S., Narteau, C., Gao, X., 2014. Two modes for dune orientation. Geology 42, 743–746.

Ewing, R., Kocurek, G., 2010. Aeolian dune-field pattern boundary conditions. Geomorphology 114, 175–187.

Fenton, L.K., 2006. Dune migration and slip face advancement in the Rabe Crater dune field, Mars. Geophys. Res. Lett. 33, L20201.

Fenton, L.K., Hayward, R.K., 2010. Southern high latitude dune fields on Mars: morphology, aeolian inactivity, and climate change. Geomorphology 121, 98–121.

Fenton, L.K., Michaels, T.I., Beyer, R.A., 2014a. Inverse maximum gross bedform-normal transport 1: how to determine a dune-constructing wind regime using only imagery. Icarus 230, 5–14.

Fenton, L.K., Michaels, T.I., Chojnacki, M., Beyer, R.A., 2014b. Inverse maximum gross bedform-normal transport 2: application to a dune field in Ganges Chasma, Mars and comparison with HiRISE repeat imagery and MRAMS. Icarus 230, 47–63.

Fenton, L.K., Toigo, A.D., Richardson, M.I., 2005. Aeolian processes in proctor crater on mars: mesoscale modeling of dune-forming winds. J. Geophys. Res., Planets 110 (E6).

Forget, F., Hourdin, F., Fournier, R., Hourdin, C., Talagrand, O., Collins, M., Lewis, S.R., Read, P.L., Huot, J.-P., 1999. Improved general circulation models of the Martian atmosphere from the surface to above 80 km. J. Geophys. Res., Planets 104, 24155–24175.

Gao, X., Narteau, C., Rozier, O., 2015a. Development and steady states of transverse dunes: a numerical analysis of dune pattern coarsening and giant dunes. J. Geophys. Res. 120, 2200–2219.

Gao, X., Narteau, C., Courrech du Pont, S., 2015b. Phase diagrams of dune shape and orientation depending on sand availability. Sci. Rep. 5, 14677.

Gardin, E., Allemand, P., Quantin, C., Silvestro, S., Delacourt, C., 2012. Dune fields on Mars: recorders of a climate change? Planet. Space Sci. 60, 314–321.

Hayward, R.K., Fenton, L., Titus, T.N., 2014. Mars global digital dune database (MGD 3): global dune distribution and wind pattern observations. Icarus 230, 38–46.

Hayward, R.K., Mullins, K.F., Fenton, L.K., Hare, T.M., Titus, T.N., Bourke, M.C., Colaprete, A., Christensen, P.R., 2007. Mars global digital dune database and initial science results. J. Geophys. Res., Planets 112, E11007.

Jackson, P.S., Hunt, J.C.R., 1975. Turbulent wind flow over a low hill. Q. J. R. Meteorol. Soc. 101, 929–955.

Kocurek, G., Lancaster, N., 1999. Aeolian system sediment state: theory and Mojave Desert Kelso dune field example. Sedimentology 46, 505–515.

Lancaster, N., 1991. The orientation of dunes with respect to sand-transporting winds: a test of Rubin and Hunter's gross bedform-normal rule. Acta Mech., Suppl. 2, 89–102.

Lancaster, N., 2010. Assessing dune-forming winds on planetary surfaces—application of the gross bedform normal concept. In: LPI Contrib., vol. 1552, pp. 39–40.

Lorenz, R., Zimbelman, J., 2014. Dune Worlds. Springer.

Lü, P., Narteau, C., Dong, Z., Rozier, O., Courrech du Pont, S., 2017. Unravelling raked linear dunes to explain the coexistence of bedforms in complex dunefields. Nat. Commun. 8, 14239.

Lucas, A., Narteau, C., Rodriguez, S., Rozier, O., Callot, Y., Garcia, A., Courrech du Pont, S., 2015. Sediment flux from the morphodynamics of elongating linear dunes. Geology 43, 1027–1030.

Lucas, A., Rodriguez, S., Narteau, C., Charnay, B., Pont, S.C., Tokano, T., Garcia, A., Thiriet, M., Hayes, A.G., Lorenz, R.D., et al., 2014. Growth mechanisms and dune orientation on titan. Geophys. Res. Lett. 41, 6093–6100.

Malin, M.C., Bell, J.F., Cantor, B.A., Caplinger, M.A., Calvin, W.M., Clancy, R.T., Edgett, K.S., Edwards, L., Haberle, R.M., James, P.B., et al., 2007. Context camera investigation on board the Mars Reconnaissance Orbiter. J. Geophys. Res., Planets 112 (E5).

Massé, M., Bourgeois, O., Le Mouélic, S., Verpoorter, C., Spiga, A., Le Deit, L., 2012. Wide distribution and glacial origin of polar gypsum on Mars. Earth Planet. Sci. Lett. 317, 44–55.

Narteau, C., Zhang, D., Rozier, O., Claudin, P., 2009. Setting the length and time scales of a cellular automaton dune model from the analysis of superimposed bed forms. J. Geophys. Res. 114, F03006.

Ping, L., Narteau, C., Dong, Z., Zhang, Z., Courrech du Pont, S., 2014. Emergence of oblique dunes in a landscape-scale experiment. Nat. Geosci. 7, 99–103.

Piqueux, S., Kleinböhl, A., Hayne, P.O., Kass, D.M., Schofield, J.T., McCleese, D.J., 2015. Variability of the martian seasonal CO_2 cap extent over eight Mars years. Icarus 251, 164–180.

Rubin, D., Hunter, R., 1987. Bedform alignment in directionally varying flows. Science 237, 276–278.

Rubin, D.M., 2012. A unifying model for planform straightness of ripples and dunes in air and water. Earth-Sci. Rev. 113, 176–185.

Rubin, D.M., Carter, C.L., 1987. Cross-Bedding, Bedforms, and Paleocurrents. SEPM.

Rubin, D.M., Tsoar, H., Blumberg, D.G., 2008. A second look at western Sinai seif dunes and their lateral migration. Geomorphology 93, 335–342.

Runyon, K., Bridges, N., Ayoub, F., Newman, C., Quade, J., 2017. An integrated model for dune morphology and sand fluxes on Mars. Earth Planet. Sci. Lett. 457, 204–212.

Silvestro, S., Fenton, L., Vaz, D., Bridges, N., Ori, G., 2010. Ripple migration and dune activity on Mars: evidence for dynamic wind processes. Geophys. Res. Lett. 37, L20203.

Smith, I.B., Spiga, A., Holt, J.W., 2015. Aeolian processes as drivers of landform evolution at the south pole of Mars. Geomorphology 240, 54–69.

Spiga, A., Forget, F., 2009. A new model to simulate the Martian mesoscale and microscale atmospheric circulation: validation and first results. J. Geophys. Res., Planets 114, E02009.

Sullivan, R., Arvidson, R., Bell, J., Gellert, R., Golombek, M., Greeley, R., Herkenhoff, K., Johnson, J., Thompson, S., Whelley, P., et al., 2008. Wind-driven particle mobility on Mars: insights from Mars Exploration Rover observations at "El Dorado" and surroundings at Gusev Crater. J. Geophys. Res., Planets 113, E06S07.

Toigo, A.D., Richardson, M.I., 2002. A mesoscale model for the Martian atmosphere. J. Geophys. Res., Planets 107, 1–21.

Toigo, A.D., Waugh, D.W., Guzewich, S.D., 2017. What causes Mars' annular polar vortices? Geophys. Res. Lett. 44 (1), 71–78. https://doi.org/10.1002/2016GL071857.

Tyler, D., Barnes, J.R., 2005. A mesoscale model study of summertime atmospheric circulations in the north polar region of Mars. J. Geophys. Res., Planets 110, E06007.

Wasson, R., Hyde, R., 1983. Factors determining desert dune type. Nature 304, 337–339.

Waugh, D.W., Toigo, A.D., Guzewich, S.D., Greybush, S.J., Wilson, R.J., Montabone, L., 2016. Martian polar vortices: comparison of reanalyses. J. Geophys. Res., Planets 121 (9), 1770–1785. https://doi.org/10.1002/2016JE005093.

Werner, B.T., Kocurek, G., 1997. Bed-from dynamics: does the tail wag the dog? Geology 25, 771–774.

Wilson, I.G., 1973. Ergs. Sediment. Geol. 10, 77–106.

Zhang, D., Narteau, C., Rozier, O., Courrech du Pont, S., 2012. Morphology and dynamics of star dunes from numerical modelling. Nat. Geosci. 5, 463–467.